On the Formation and Collimation of an Axially-Symmetrical Hollow Electron Beam

By

LEONARD CALDWELL ADAMS

A DISSERTATION PRESENTED TO THE GRADUATE COUNCIL OF
THE UNIVERSITY OF FLORIDA
IN PARTIAL FULFILLMENT OF THE REQUIREMENTS FOR THE
DEGREE OF DOCTOR OF PHILOSOPHY

UNIVERSITY OF FLORIDA
January, 1956

ACKNOWLEDGMENT

The author wishes to express his sincere gratitude to all members of the supervisory committee, both former and present, for their continued guidance and encouragement in this endeavor. He is especially indebted to Dr. E. E. Muschlitz, Jr., who contributed immeasurably of his academic and practical skills during the experimental work and preparation of the dissertation.

TABLE OF CONTENTS

Page

LIST OF TABLES v

LIST OF ILLUSTRATIONS vi

Chapter

I. INTRODUCTION 1

II. THEORY RELATING TO BEAM DESIGN 3

- Conditions in the Cathode Region
- Conditions in the Transition Region
- Interpretation of Magnetic Potential in Terms of Flux
- Nature of Ψ as a Function of z

III. QUALITATIVE PRESENTATION OF TUBE DESIGN . 20

- Pierce Electron Gun Approach to Cathode Region - Analogue Method
- Approach to Magnetic Field Distribution
- Approach to Transition Region Design

IV. DESCRIPTION OF EXPERIMENTS 31

- Location of Focusing Electrodes in Cathode Region
- Determination of Magnetic Flux Distribution
- Locating Electrodes in the Transition Region
- Description of Hollow Beam Electron Gun and Collimating Device
- Tube-Test Procedure and Results

V. SUMMARY 53

APPENDIX I. THE NET-POINT EQUATION 57

APPENDIX II. ON THE ELECTROLYTIC TANK ANALOGY . . 60

TABLE OF CONTENTS (continued)

Page

APPENDIX III. ON FLUX PLOTTING 64

BIBLIOGRAPHY 68

BIOGRAPHY 70

LIST OF TABLES

Table | Page

1. Potentials Observed in the Electrolytic Tank Analogue 33
2. Tube Element Identification 46
3. Tube Test Data 47
4. Collimation Data 51

LIST OF ILLUSTRATIONS

Figure		Page
2.1	Regions of the Electron Beam	4
2.2	Hollow Beam Immersed in an Infinite Diode .	4
2.3	The Magnetic Field and the Electron Beam in the Transition Region	12
2.4	Differential Quantity of Flux Passing Through a Differential Area	12
2.5	Flux vs. Axial Distance in the Transition Region	19
3.1	Tank Scheme for Solution in the Cathode Region	23
3.2	Typical Electrode Positions	23
3.3	Tank Arrangement for Taking Magnetic Field Data	25
3.4	Typical Potential Distribution Along the Beam	28
3.5	Net-Points Outside the Beam	29
4.1	Focusing Electrode System for the Cathode Region	32
4.2	Map of the Magnetic Field	35
4.3	Flux vs. Axial Distance in the Transition Region	36
4.4	Flux Density vs. Solenoid Current	36
4.5	Representing Points Used in Sample Calculations	38

LIST OF ILLUSTRATIONS (continued)

Figure Page

4.6 Map of Electric Potential Field in the Charge Free Region 41

4.7 Cross-Section of the Hollow Beam Electron Gun 42

4.8 The Electron Gun and Test Set-Up 52

CHAPTER I

INTRODUCTION

Electron beams having high space-charge density are of great importance in the operation of traveling-wave amplifier and oscillator tubes. Those designs which have been most successful have employed axially symmetrical beams, and a considerable amount of work has been done in studying the properties of such beams.[1-5*]

In the main, these tubes have employed solid beams with an axially long interaction space (the name commonly used to refer to the region of interaction between electron beam and traveling electromagnetic wave). To maintain a relatively constant beam radius extremely strong axial magnetic fields are ordinarily employed. In fact, an infinite field is frequently assumed in theoretical analyses to render difficult problems soluble.

This work is concerned with hollow cylindrical beams collimated by a weak radial magnetic field in conjunction with electric field focusing. Harris[5] has demonstrated that hollow electron beams, having a rotational as well as an axial motion,

---

[*] Superscript numerals refer to Bibliography.

can be maintained without an axial magnetic field. Then if such a beam were formed and properly introduced into the interaction region, the tube would operate with a great saving of beam and magnetic field energy.

Tangential velocities are given to the electrons for two purposes. First, assuming that collimation is possible, the spiral trajectory provides a long interaction space in a relatively short axial length. The slow-wave guiding structure can be wound about the beam as a helix having the same pitch as the electron trajectory. Thus collimation over great lengths becomes unnecessary. Second, the centrifugal forces are useful in the collimation problem, particularly at the inner beam radius.

In view of the desirable applications, the purpose of this effort is a study of the dense, hollow beam problem. A design technique for an electron gun and collimating device is offered, and the results of tests on an experimental model are presented and interpreted.

Chapter II deals with a general theory of beam design. Consideration is given to beam conditions near the cathode and in the magnetic flux regions separately. Chapter III is concerned with the theoretical aspects of design techniques as applied to the particular problem of this paper. In Chapter IV quantitative information is presented along with a description of experiments and interpretation of experimental results.

CHAPTER II

THEORY RELATING TO BEAM DESIGN

The electron beam discussed here is of hollow cylindrical geometry, having about the same size as a one-inch water pipe. The over-all length of the beam is about two and one-half centimeters. For convenience of analysis the beam is considered to exist in two regions. First, the cathode region is a space of about one centimeter in which no magnetic field exists. In this region the current is space-charge-limited, and Child's law is assumed to apply. Second, the transition region begins after the beam passes through an anode opening at the extremity of the cathode region. In the transition region the beam passes through a radial magnetic field and achieves angular velocity. Figure 2.1 depicts these divisions.

Conditions in the Cathode Region

Design in the cathode region is a special application of the Pierce electron-gun technique.[6] In general, this procedure assumes that if we remove all of an infinite beam except the desired portion, and establish the same field and potential values existing in the infinite case along the

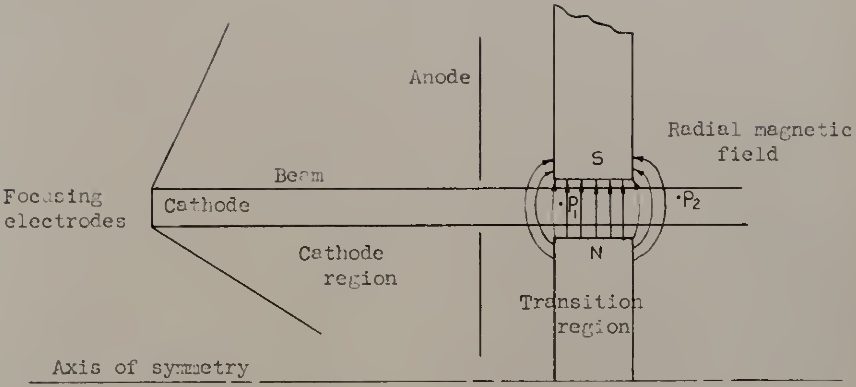

REGIONS OF THE ELECTRON BEAM

FIGURE 2.1

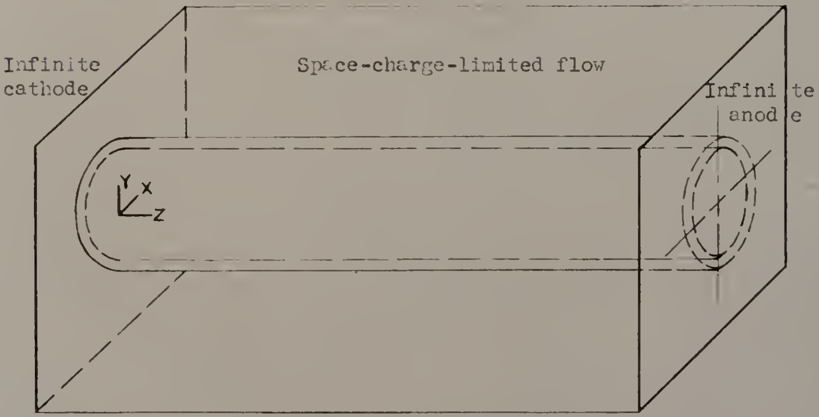

HOLLOW BEAM IMMERSED IN AN INFINITE DIODE

FIGURE 2.2

boundaries of the desired portion, then the desired portion will remain collimated.

Consider Figure 2.2. This represents a section between infinite parallel planes, one of which is a cathode and the other an anode with space-charge-limited current flow between. The cylinder, shown in dark lines, represents the beam geometry we would like to select from the infinity of charge. Clearly, the component of electric field normal to the surface of the cylinder is zero. Therefore, if the cylinder is isolated from the remainder of the charge, one condition on its equilibrium is:

$$\frac{\delta \phi}{\delta r} = 0 \quad \text{at } r = r_a \text{ and } r = r_b, \tag{2.1}$$

where ϕ is the electric potential in volts

r is the radial coordinate in meters

a and b designate bounding radii.

The other condition for equilibrium of the cylinder is that it have the axial potential distribution of the infinite beam. To find this we make an application of Child's law which, in its usual form, states that the current density in the space-charge-limited case is directly proportional to the three-halves power of potential and inversely proportional to the second power of anode-cathode spacing. For the sake of completeness a derivation of the law giving potential as a function of spacing is included here.[7]

For this case potential varies only in the z-direction and Poisson's equation becomes

$$\frac{d^2\phi}{dz^2} = -\frac{\rho}{\epsilon_o}, \qquad (2.2)$$

where ρ is the charge density in coulombs per cubic meter

ϵ_o is the permittivity of free space in farads per meter.

Current continuity requires that

$$J = -\rho v, \qquad (2.3)$$

where J is electron current density in amperes per square meter

v is charge velocity in meters per second.

We shall also need the energy conservation equation which for the case of zero cathode potential, states that

$$e\phi = -\frac{1}{2} mv^2, \qquad (2.4)$$

where e = -1.602 x 10^{-19} coulombs, the electronic charge

m = 9.11 x 10^{-31} kilograms, the electronic mass.

Solving equation 2.4 for v, equation 2.3 for ρ and substituting in 2.2 we obtain

$$\frac{d^2\phi}{dz^2} = \frac{J}{\epsilon_o} \sqrt{-\frac{m}{2e}}\, \phi^{-1/2} .$$

Multiply this through by $2\frac{d\phi}{dz}$ to obtain the integrable form,

$$\int \frac{d^2\phi}{dz^2}\, 2\frac{d\phi}{dz}\, dz = \frac{2J}{\epsilon_o}\sqrt{-\frac{m}{2e}}\int \phi^{-1/2}\, d\phi .$$

Integrating,

$$\left(\frac{d\phi}{dz}\right)^2 = \frac{4J}{\epsilon_o}\sqrt{-\frac{m}{2e}}\,\phi^{1/2} + C_1 . \tag{2.5}$$

For the space-charge-limited case the potential and electric field are zero at the cathode. Hence C_1 is zero. Taking the square root of both sides of equation 2.5 and integrating again yields

$$\phi^{3/4} = \frac{3}{2}\sqrt{\frac{J}{\epsilon_o}}\,\sqrt[4]{-\frac{m}{2e}}\; z + C_2 .$$

Zero cathode potential requires that C_2 be zero, so finally

$$\phi = \left(\frac{3}{2}\right)^{4/3}\left(\frac{J}{\epsilon_o}\right)^{2/3}\left(-\frac{m}{2e}\right)^{1/3} z^{4/3} . \tag{2.6}$$

Equation 2.6 states that for a dense beam having current density J, the potential at all points along the beam is determined by

$$\phi = Kz^{4/3} . \tag{2.7}$$

Equations 2.7 and 2.1 satisfied at radii a and b are the necessary and sufficient conditions that the hollow beam be collimated in the cathode region. The electrode system must be capable of producing these conditions with the beam present.

Note that in the derivation of 2.7 the current density was treated as a constant. A notable exception to this assumption is shot noise.[7] This effect is due to the tendency of cathodes to emit electrons in "bunches" rather than in continuous flow. However, the space-charge has an absorbing effect on these bursts of charge and minimizes current density variations. This is one of the reasons for using high electron densities in the tube.

Conditions in the Transition Region

The electrons are focused in the cathode section of the gun and are accelerated to the desired velocity by an anode operating at an appropriate potential. The anode has a circular opening which permits the beam to pass into the transition region. In this section of the tube the electrons are caused to pass through a steady, radial, magnetic field. In so doing they receive an angular component of velocity which is very important in this tube from two standpoints. First, it is the purpose of a gun of this type to provide a dense beam with a long interaction path in order that maximum utility may be made of the tube. Beam rotation requires an individual electron to travel along a spiral trajectory, thus stretching its interaction space to several times the linear length of the beam. Second, the centrifugal forces experienced by the electrons turn out to be quite useful in the collimation problem.

In what follows the differential equations pertinent to transition region design are developed. Lagrange's equation states that

$$\frac{d}{dt}\left(\frac{\delta L}{\delta \dot{q}_i}\right) - \frac{\delta L}{\delta q_i} = 0, \tag{2.8}$$

where $L = (T - U)$, the Lagrangian

T = Kinetic energy of the particle

U = Potential energy of the particle such that $F = -\nabla U$ is a conservative force field

q_i is the i^{th} coordinate of the particle

$\dot{q}_i$ is the total time derivative of the i^{th} coordinate.

The kinetic energy, T, of any given electron is simply

$$T = \frac{1}{2}mv^2.$$

The potential energy, U, is not so easily expressed. It is not electric potential but a potential such that its gradient is a force. In the absence of magnetic flux

$$U = e\phi, \tag{2.9}$$

where e, the electron charge, is to be considered a negative number. This leads to the proper force field since

$$F = -\nabla U = -e(\nabla\phi) = eE.$$

E represents the conventional electric field. When the moving electron enters a magnetic field, a new component of force is encountered.

$$\overline{F_m} = e(\bar{v} \times \bar{B}) \qquad (2.10)$$

where $\overline{F_m}$ is the component of force due to the magnetic field

$\bar{B}$ is the density of the magnetic field.

The total force on the electron is then

$$\begin{aligned} \bar{F} &= -e\nabla\phi + e(\bar{v} \times \bar{B}) \\ &= -e(\nabla\phi - \bar{v} \times \bar{B}). \end{aligned} \qquad (2.11)$$

Let us postulate that the above equation may be written

$$F = -e(\nabla\phi + \nabla\phi') = -\nabla U, \qquad (2.12)$$

where ϕ', as well as ϕ, is a proper potential function. Note that this is equivalent to assuming that ϕ' exists such that

$$\nabla\phi' = -\bar{v} \times \bar{B}. \qquad (2.13)$$

Such a potential does exist[9] and is defined by the equation

$$\phi' = -\bar{v}\cdot\bar{A}, \qquad (2.14)$$

where $\bar{v}$ is vector velocity.

$\bar{A}$ is the vector potential of the magnetic field; i.e., $\bar{B} = \nabla \times \bar{A}$. Finally, the Lagrangian is applicable and it takes the form

$$L = \frac{1}{2} mv^2 - (e\phi + e\phi') \qquad (2.15)$$

$$= \frac{1}{2} mv^2 - e\phi + e(\bar{v} \cdot \bar{A}).$$

This classical, general equation is now applied to the problem at hand, making use of cylindrical coordinates. Refer to Figure 2.3. The most general vector velocity of a given electron is

$$\bar{v} = 1_r\dot{r} + 1_\theta r\dot{\theta} + 1_z\dot{z} ,$$

where 1_r, 1_θ, and 1_z are the unit vectors of the coordinate system. The flux density vector has only a radial component*; hence the magnetic potential is

$$\bar{A} = 1_\theta A_\theta .$$

Substitution of these values in equation 2.15 gives

$$L = \frac{1}{2} m(\dot{r}^2 + r^2\dot{\theta}^2 + \dot{z}^2) - e\phi + er\dot{\theta}A_\theta . \qquad (2.16)$$

Lagrange's equation is applied to this expression to find the conditions for beam equilibrium.

For the r- coordinate we find that

$$m\ddot{r} = mr\dot{\theta}^2 - e\frac{\delta\phi}{\delta r} + e\dot{\theta}\frac{\delta}{\delta r} (rA_\theta); \qquad (2.17)$$

---

*This is explained in the following section.

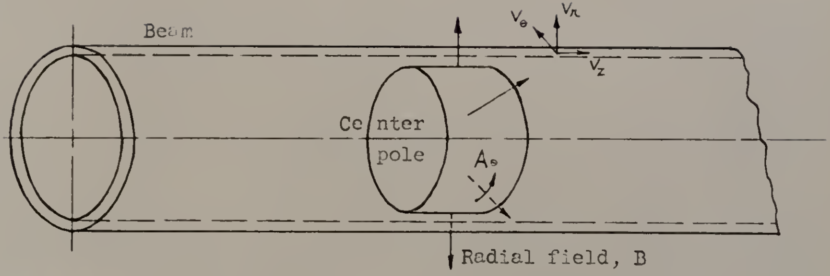

THE MAGNETIC FIELD AND THE ELECTRON BEAM IN THE TRANSITION REGION

FIGURE 2.3

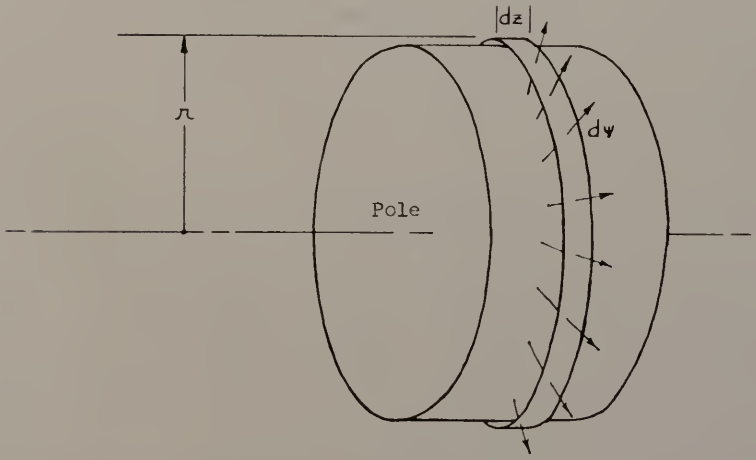

DIFFERENTIAL QUANTITY OF FLUX PASSING THROUGH A DIFFERENTIAL AREA

FIGURE 2.4

for the θ-coordinate,

$$mr^2\dot{\theta} = -erA_\theta + C_3; \qquad (2.18)$$

and for the z- coordinate,

$$m\ddot{z} = -e\frac{\delta \phi}{\delta z} + e\dot{\theta}\frac{\delta}{\delta z}\,(rA_\theta). \qquad (2.19)$$

Equations 2.17, 2.18, and 2.19 constitute the design requirements for the beam. The utility of these expressions is clarified in the next section.

Interpretation of Magnetic Potential in Terms of Flux

Magnetic vector potentials are easily defined mathematically.[10] They are not, however, easy to visualize. In general, they have the direction of currents which establish the field. Where currents are absent one may imagine a current direction which could have produced the field.

The magnetic field cut by the beam in this tube is radial. It is established by two concentric pole pieces with a circular gap. The magnetic potential is defined by

$$\overline{B} = \quad \times \overline{A} \qquad (2.20)$$

Since $\overline{B}$ is radial and axially symmetrical, the vector $\overline{A}$ need only have a tangential component. Assume this is the case and consider an expansion of equation 2.20.

$$\begin{aligned} &r\text{ - component } \overline{B} = B_r = -\frac{\delta A_\theta}{\delta z} \\ &\theta\text{ - component } B_\theta \equiv 0 \qquad\qquad (2.21) \\ &z\text{ - component } B_z = 0 = \frac{\delta}{\delta r}(rA_\theta) \end{aligned}$$

The equations 2.21 suggest that $A_\theta = \frac{1}{r}f(z)$. In what follows this is verified, and the particular solution of interest in this paper is found. Figure 2.4 shows how the flux density may be expressed in a manner most applicable to this problem. Clearly, the flux density is given by

$$\overline{B} = B_r = \frac{d\Psi}{da} = \frac{1}{2\pi r}\,\frac{d\Psi}{dz} \qquad (2.22)$$

where Ψ is the flux traversed by the beam as it progresses in the transition region. Substituting this result in the first of the equations 2.21 yields

$$\frac{1}{2\pi r}\,\frac{d\Psi}{dz} = -\frac{\delta A_\theta}{\delta z},$$

or

$$d\Psi = -2\pi\frac{\delta}{\delta z}(rA_\theta)dz.$$

But in view of axial symmetry and the third of the equations 2.21, all derivatives of the quantity (rA_θ), except with respect to z, are zero; hence $\frac{\delta}{\delta z}(rA_\theta)dz$ is the total differential, $d(rA_\theta)$. Therefore,

$$\Psi = -2\pi r A_\theta + C_4 \qquad (2.23)$$

When the beam has passed completely through the field, it has traversed the total flux, which we shall call Ψ_c, and is in a region of zero magnetic potential. Introducing this boundary condition evaluates C_4.

$$C_4 = \Psi_c .$$

Thus,

$$A_\theta = \frac{1}{2\pi r}(\Psi_c - \Psi). \qquad (2.24)$$

Now substitute 2.24 in 2.18 to obtain

$$mr^2\dot{\theta} = -\frac{e}{2\pi}(\Psi_c - \Psi) + C_3 .$$

Before cutting of flux begins (i.e., $\Psi = 0$) the angular velocity is zero and

$$C_3 = \frac{e}{2\pi}\Psi_c .$$

This leads to the result,

$$\dot{\theta} = \frac{e}{m}\,\frac{\Psi}{2\pi r^2} . \qquad (2.25)$$

Equation 2.25 is recognized as Busch's Theorem applied to the geometry and problem at hand. It was found in 2.21 that $\frac{\delta}{\delta r}(rA_\theta) = 0$. Substituting this result and equation 2.25 in 2.17 yields

$$m\ddot{r} = mr\left(\frac{e}{m}\,\frac{\Psi}{2\pi r^2}\right)^2 - e\frac{\delta\emptyset}{\delta r} .$$

For collimation it is required that there be no radial acceleration at the beam boundaries. Calling these values of radii r_o, the above equation requires that

$$\left(\frac{\delta \phi}{\delta r}\right)_{r_o} = \frac{e}{m}\left(\frac{\Psi^2}{4\pi^2 r_o{}^3}\right) \tag{2.26}$$

Equation 2.26 is a most significant one. It specifies the value of the radial component of electric field at beam boundaries in terms of flux traversed. To complete the boundary conditions the potential ϕ must also be specified. This is accomplished by substituting 2.25 in the energy conservation equation,

$$e\phi = -\frac{1}{2}m(\dot{r}^2 + r^2\dot{\theta}^2 + \dot{z}^2). \tag{2.27}$$

At boundaries the electrons are permitted no radial velocity, therefore

$$(\phi)_{r_o} = -\frac{1}{2}\frac{m}{e}\left[r_o{}^2 \frac{e^2\Psi^2}{m^2 4\pi^2 r_o{}^4} + (\dot{z})^2_{r_o}\right],$$

or

$$(\phi)_{r_o} = -\frac{1}{8}\frac{e\Psi^2}{m\pi r_o{}^2} - \frac{1}{2}\frac{m}{e}(\dot{z})^2_{r_o} . \tag{2.28}$$

Equations 2.25, 2.26, and 2.28 might be considered the beam design conditions. Similar relations were suggested by Harris[5], derived in a somewhat different manner. The derivations are included here for completeness and to give further insight into the solution of the collimation problem.

At first it would seem that 2.28 leaves us in something of a dilemma because of its dependence upon $\dot{z}$.

Actually, this is not the case. Simply specify $(\emptyset)_{r_o}$ as a function of z and let $(\dot{z})_{r_o}$ as a function of z be what it will. This procedure is possible because $\left(\frac{\delta\emptyset}{\delta r}\right)_{r_o}$ is independent of $(\emptyset)_{r_o}$. Certainly an initial velocity in the axial direction must be imparted to the beam, and this velocity must be maintained great enough to keep shot noise subdued. Also, if the tube is to be of practical value the beam must progress axially after emerging from the transition region. The selection of a function for $(\emptyset)_{r_o}$ and the reasons therefor are presented in Chapter III.

Both $\dot{z}$ and $\dot{\theta}$ must be known in order to utilize the beam because the helical trajectory is specified. Equation 2.25 gives $\dot{\theta}$. The value of $\dot{z}$ follows readily from the law of conservation of energy. Upon emerging from the transition region,

$$e(\emptyset)_{r_o} = -\frac{1}{2}m\left[{r_o}^2\dot{\theta}^2 + (\dot{Z})^2_{r_o}\right].$$

Knowing $\dot{\theta}$ and having specified $(\emptyset)_{r_o}$ we have $(\dot{z})_{r_o}$ implicitly. Its value could be found similarly at any point in the transition region, but there seems to be little reason for this.

Nature of Ψ as a Function of z

An ideal transition region would be one with all of the magnetic flux concentrated in a very short axial distance. This is impossible to achieve, however, and in practice the flux distribution is somewhat like that shown in Figure 2.1

In the terminology of preceding mathematical development the total flux passing from the inner to the outer pole section is Ψ_c. Thus a beam segment at point P_2 would have cut Ψ_c flux lines, a beam segment at P_1 would have cut Ψ_1 and so on. Figure 2.5 shows a typical curve of flux versus distance through the transition region. This is an empirical function and it may be found by flux-plotting or analogue methods. One method for doing this is discussed in a later chapter.

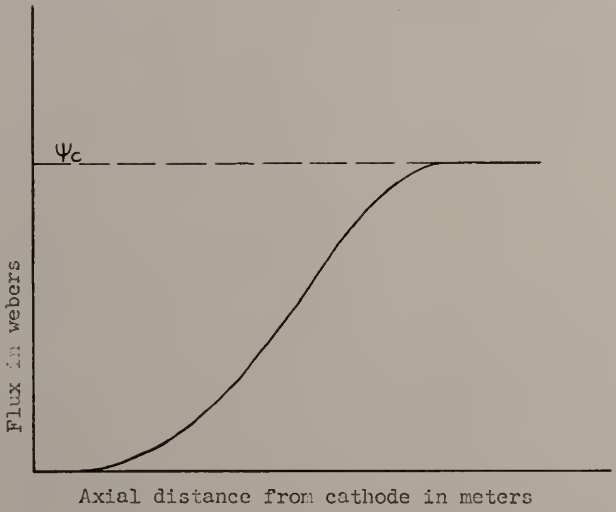

TYPICAL CURVE OF FLUX VERSUS AXIAL DISTANCE IN THE TRANSITION REGION

FIGURE 2.5

CHAPTER III

QUALITATIVE PRESENTATION OF TUBE DESIGN

Pierce Electron Gun Approach to Cathode Region - Analogue Method

This study was made simultaneously with a separate study dealing with the application of a hollow cylindrical electron beam in a specific traveling-wave amplifier tube. The amplifier tube in itself is related to this work only insofar as specifications of physical dimensions and working potentials are concerned. It was required that the beam-forming and collimating device provide a 100 milliampere stream of electrons confined to an inner radius of 1.3 centimeters and an outer radius of 1.64 centimeters. The maximum beam potential in the cathode region was specified at 720 volts.

Thus, cathode region design for this particular tube is resolved into the problem of finding proper electrode shapes and spacings to establish a $\frac{4}{3}$ power variation of potential along the beam edges, to impart 720 electron volts of energy to the particles, and to maintain the beam formation. An electrolytic tank analogy is employed for the solution.[6]

Application of the electrolytic tank to static field problems having axial symmetry is accomplished by tilting the tank through a small angle. See Figure 3.1. The wedge of electrolyte thus formed simulates a section of the complete cylinder. Current flow lines in the electrolyte create a potential-drop field which satisfies Laplace's equation as does the true potential field in the tube. The intersection of the edge of the electrolyte with the bottom of the tank creates a line representing the axis of the system.

The conditions which must be met at both inside and outside boundary surfaces of the beam are:

$$\frac{\delta \emptyset}{\delta r} = 0. \qquad (3.1)$$

$$\emptyset = KZ^{4/3}. \qquad (3.2)$$

Condition 3.1 is established in the analogue by erecting an insulating strip parallel to the axis at a radius representing the edge of the beam. This assures no current flow in a direction normal to the boundary. (See element (b), Figure 3.1.) Condition 3.2 is established by adjusting the focusing electrodes. This is a trial and error process. In the actual design it was found that two properly shaped and spaced conducting surfaces serve adequately. In general, however, as many electrodes as necessary might be employed. The cathode end (at a) is operated at zero potential and the extreme end at any convenient potential to represent tube operating level. Shaping and positioning of the surfaces are then adjusted until one reads values of potential along the insulating strip in agreement with equation 3.2. Electrode shapes on the inside beam edge are found similarly, the difference being that conducting surfaces are erected on the opposite side of the dielectric strip, and the strip is moved to a radius corresponding to the inner boundary of the beam. Measurements are made using a potentiometer arrangement so as to insure no current flow to the probe. The system is scaled such that the surface area of the electrolyte is large compared with the configuration of the analogue. Figure 3.2 depicts a cross-section view of typical electrodes found in the above described manner.

Approach to Magnetic Field Distribution

Flux plotting and analogue methods of locating magnetic field lines are widely described in literature[6,7,10], so only facts pertinent to the design of this tube will be presented here.

Reference to Figure 2.1 shows the general arrangement of the radial field in the tube, and reference to the section on Interpretation of Magnetic Potential (Chapter II) points out the necessity for an accurate knowledge of the

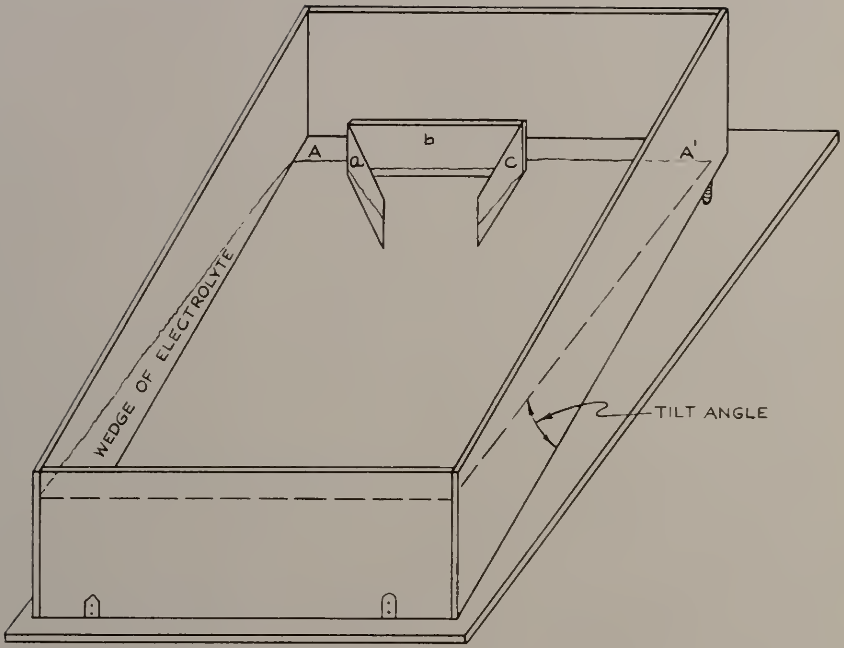

TANK SCHEME FOR SOLUTION IN CATHODE REGION

FIGURE 3.1

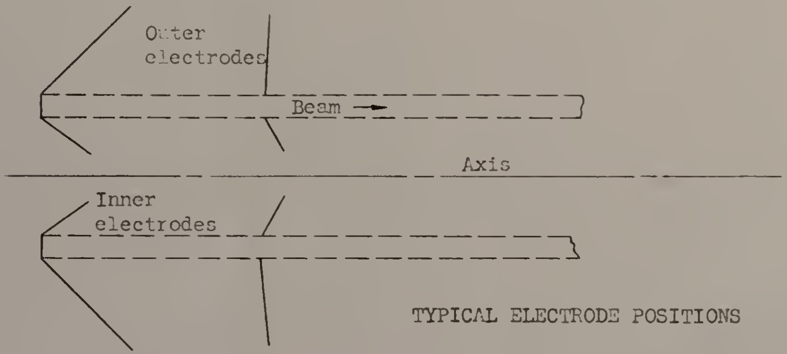

TYPICAL ELECTRODE POSITIONS

FIGURE 3.2

distribution of the field. Figure 3.3 shows a top view of the arrangement in the tank for taking magnetic field data.

Notice that this data provides equipotential lines. The actual flux distribution is a family of curves orthogonal to the equipotentials. The flux lines are found by sketching in the perpendicular set, employing the curvilinear square principle. When the flux plot is found, one can correctly assume that all flux passes between the extreme lines and that an equal amount is contained in each tube defined by adjacent lines. By making an accurate plot with a large number of tubes a uniform function of flux versus axial distance is determined. Figure 2.5 shows such a function. Actual experimental results are presented in Chapter IV.

Approach to Transition Region Design

It is assumed that the hollow cylindrical beam enters the transition region well collimated. In this region the electrons cross a radial magnetic field and obtain tangential components of velocity. It is the purpose of this section to determine an electrode configuration to maintain collimation. The equations for equilibrium in the transition region are:

$$\left(\frac{\delta \phi}{\delta r}\right)_{r_o} = \frac{e}{m} \frac{\Psi^2}{4\pi r_o{}^3} \qquad (2.26)$$

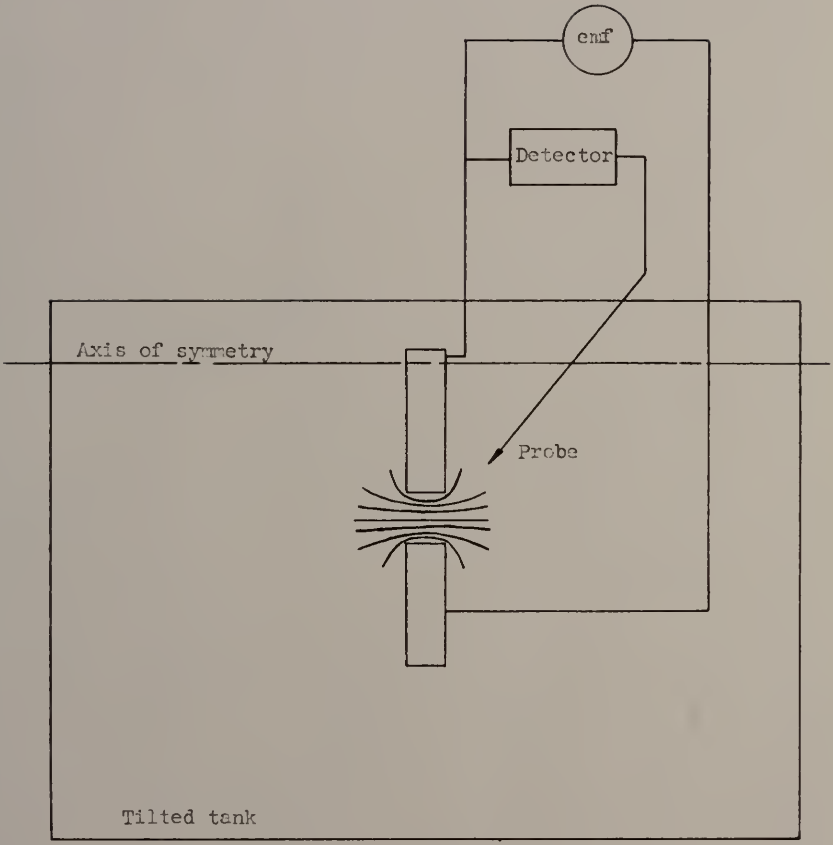

TANK ARRANGEMENT FOR TAKING MAGNETIC FIELD DATA

FIGURE 3.3

and

$$(\phi)_{r_o} = -\frac{e}{m}\,\frac{\Psi^2}{8\pi r_o^{\,2}} - \frac{m(\dot{z})^2 r_o}{e\;2} \quad , \qquad (2.28)$$

where r_o is either bounding radius of the beam. As mentioned earlier, the value of $(\phi)_{r_o}$ as a function of z is somewhat arbitrary. It is well, at this point, to consider the restraints on the selection of the function.

1. The function must be continuous all along the beam.
2. It must permit the beam to emerge with the proper ratio of tangential to axial velocity.
3. It must lead to a physically realizable focusing electrode system.
4. Final beam potential is specified.
5. Beam radius must remain constant.

This last condition was applied in the derivation of the design equations and must be adhered to. Conditions 2, 4, and 5 together specify the total flux, since from 4

$$v_c^{\,2} = -\,2\frac{e}{m}\phi_c ,$$

from 2

$$\frac{r_o\dot{\theta}_c}{v_c} = \text{specified constant},$$

and from 2.25

$$\dot{\theta}_c = \frac{e}{m}\,\frac{\Psi_c}{2\pi r_o^{\,2}} \quad .$$

In these equations the subscript c implies final values upon emerging from the transition region. With final potential and total flux fixed, the final value of $(\dot{z})_{r_o}$ is fixed. The choice of the function $(\phi)_{r_o}$ is arbitrary to the extent that it does not matter where the beam reaches the final energy level. It seems logical that conditions 1 and 3 might be best satisfied by a constant potential ϕ_o throughout the transition region with the curve extended smoothly into the potential function back in the cathode region. Certainly this simplifies the numerical solution to Laplace's equation in the charge-free space about the beam. For these reasons a constant value for $(\phi)_{r_o}$ is used in this particular solution to the problem. Figure 3.4 illustrates the assignment of potential values at beam radius $r_o = r_a$.

The normal derivative of potential at $r_o = r_a$ is specified by equation 2.26. Empirical relations are involved, so we resort to a net-point solution. Consider Figure 3.5. The charge-free space at radii greater than r_a is considered to be filled with an orderly array of equally-spaced points. The net is chosen as fine as practicable to minimize error. For each point along r, a potential point is calculated using equation 2.25.

$$(\phi)_{r_1} \approx (\phi)_{r_a} + \left(\frac{\delta\phi}{\delta r}\right)_{r_a} h = (\phi)_{r_a} + \frac{e}{m}\,\frac{\Psi^2 h}{4\pi^2 r_a{}^3}\,, \qquad (3.3)$$

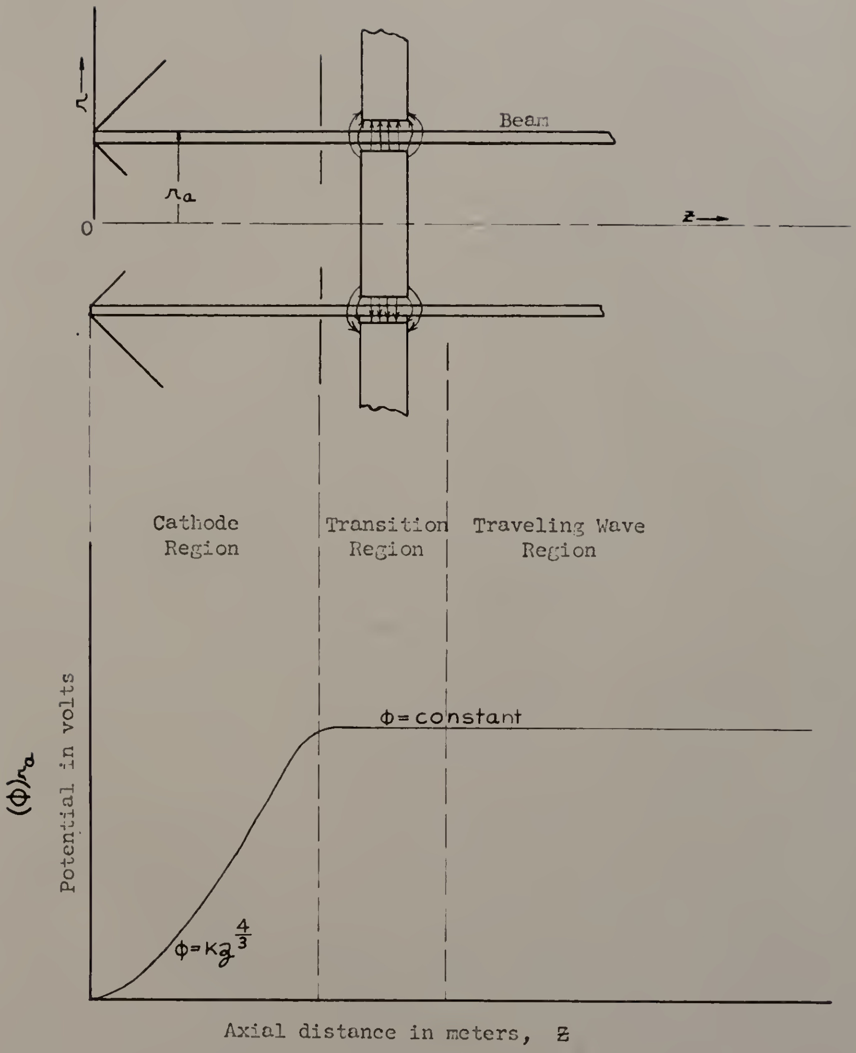

TYPICAL POTENTIAL DISTRIBUTION ALONG THE BEAM

FIGURE 3.4

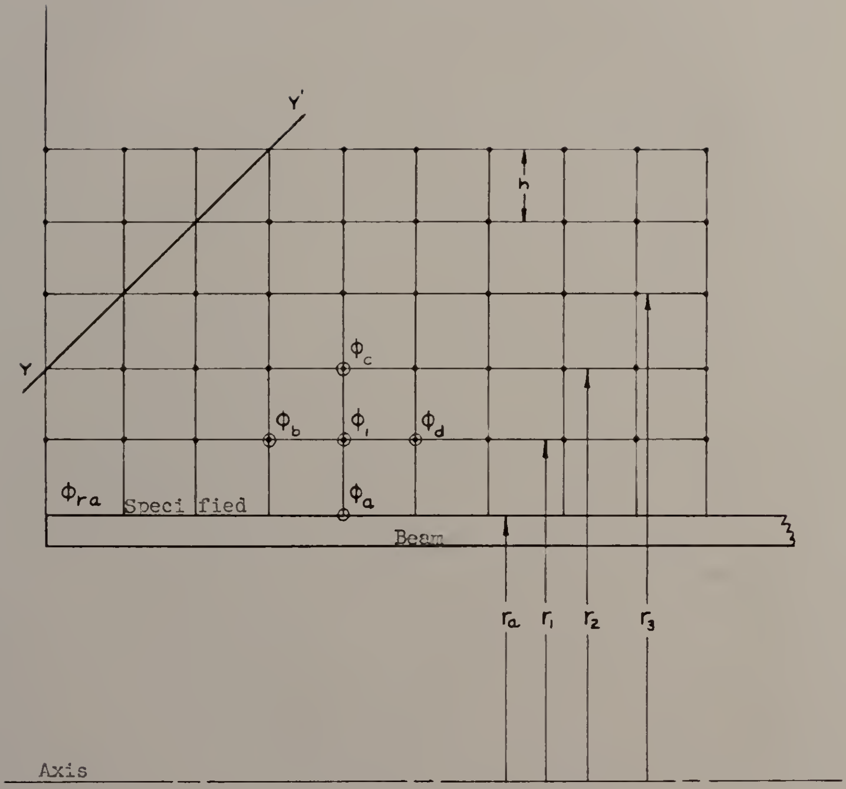

NET-POINTS OUTSIDE THE BEAM

FIGURE 3.5

where h = point spacing.

The net-point equation applicable to cylindrical coordinates with axial symmetry is:

$$\emptyset_1 = \frac{1}{4}(\emptyset_a + \emptyset_b + \emptyset_c + \emptyset_d) + \frac{h}{8r_1}(\emptyset_c - \emptyset_a),^{*} \qquad (3.4)$$

where the symbols have the significance shown in Figure 3.5. All terms in this equation are known except $\emptyset_c$. Solving for $\emptyset_c$ we have:

$$\emptyset_c = \frac{8r_1}{2r_1+h}\,\emptyset_1 - \frac{2r_1}{2r_1+h}(\emptyset_b + \emptyset_d) - \frac{2r_1-h}{2r_1+h}\,\emptyset_a. \qquad (3.5)$$

With equation 3.5 potentials for all points at radius r_1 may be determined. The author has concluded that, inasmuch as this is an approximate procedure, it is wise to plot the results in accordance with a smooth curve drawn through the average of the points. Some of these results are presented in Chapter IV. Having determined the line of potentials at r_2, the entire procedure is moved up one step and potentials are calculated for points at r_3. Note that the first point is lost each time, so there is a region behind the line y-y' (see Figure 3.5) for which we have no solution. This is of little consequence, however. We have only to fix the electrode system along equipotentials excluding this region.

---

[*] See Appendix I for a discussion of equation 3.4.

CHAPTER IV

DESCRIPTION OF EXPERIMENTS

Location of Focusing Electrodes in Cathode Region

The tube designed and tested in these experiments was required to deliver a 100 ma beam at a total potential of 720 volts. The inside radius was required to be 1.302 centimeters and the outside radius 1.640 centimeters. A suitable scale was selected and the analogy set up as described in the first section of Chapter III. Plain tap water was used as an electrolyte with a small amount of detergent to insure proper wetting of surfaces. Electrodes were of .010-inch polished copper leaf, and the beam boundaries were simulated using a vertical strip of plexiglass waxed to the tank floor. After a number of trials using several electrodes, it was concluded that two properly formed surfaces would do nicely. Figure 4.1 depicts the data obtained for the most satisfactory run. Shown dotted on this figure are spacings for two less accurate runs. Table 1 shows a comparison of potentials found in this manner with the desired beam potentials. The parenthetical numbers refer to electrode locations for a specific run.

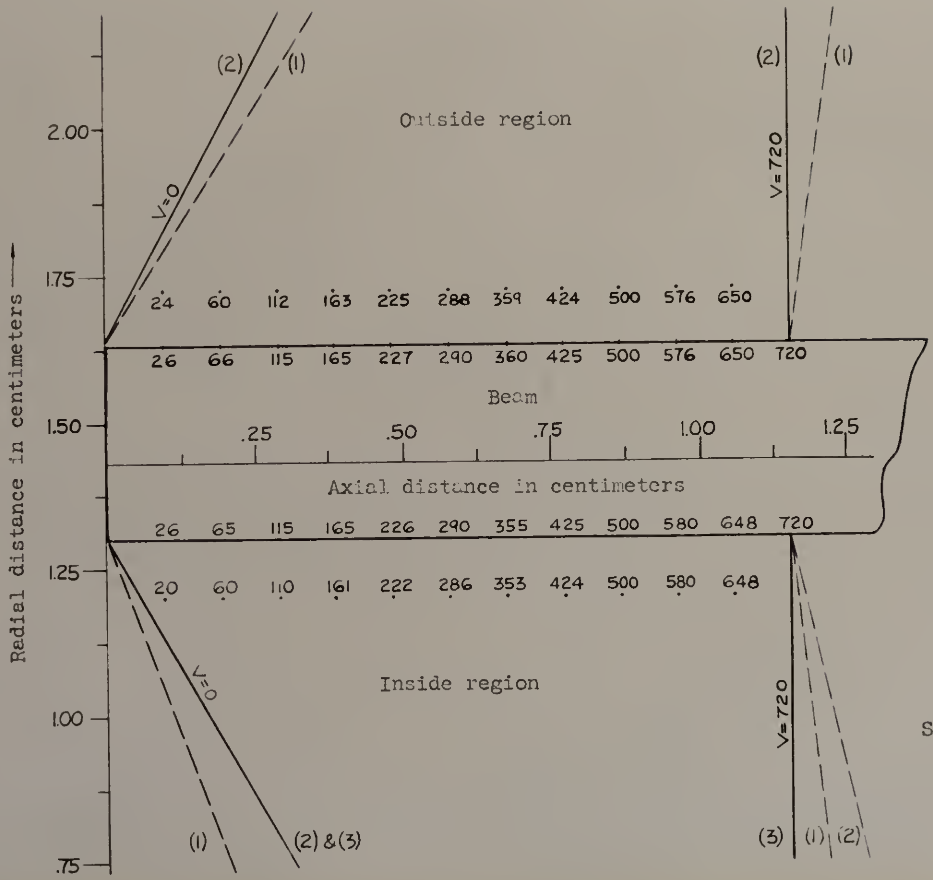

FOCUSING ELECTRODE

SYSTEM FOR THE CATHODE REGION

FIGURE 4.1

Table 1

POTENTIALS OBSERVED IN THE ELECTROLYTIC TANK ANALOGUE

Axial Distance	Ideal Potentials	Inside Potentials, volts			Outside Potentials, volts	
meters	volts	Run (1)	Run (2)	Run (3)	Run (1)	Run (2)
0	0	0	0	0	0	0
.001	26.6	30.0	26.2	26.0	24.0	26.0
.002	67.0	70.0	62.5	65.0	63.0	66.0
.003	115.0	125.0	110.5	115.0	113.0	115.0
.004	169.0	180.0	162.0	165.0	165.0	165.0
.005	228.0	230.0	225.0	226.0	225.0	227.0
.006	290.0	300.0	290.0	290.0	285.0	290.0
.007	357.0	360.0	355.0	355.0	352.0	360.0
.008	425.0	425.0	425.0	425.0	420.0	425.0
.009	500.0	500.0	500.0	500.0	500.0	500.0
.010	575.0	560.0	560.0	580.0	573.0	576.0
.011	653.0	650.0	650.0	648.0	650.0	650.0
.012	720.0	720.0	720.0	720.0	720.0	720.0

Potential values are shown on Figure 4.1 for the most desirable runs. Note that at both beam boundaries the radial component of electric field is very nearly zero. Where it has a non-zero value it is directed away from the beam. This insures focusing within the bounding radii.

Fabrication of actual tube electrodes is discussed in a later section.

Determination of Magnetic Flux Distribution

The method for taking magnetic field data is discussed in Chapter III. Figure 4.2 shows the results of data taken in this manner, and Figure 4.3 depicts the flux as a function of axial distance. In the actual tube the total flux employed was 6.2 x 10^{-6} webers, an amount necessary to give the beam the required spiral pitch.

In order to be sure that the tube was operating at the required flux value it was necessary to obtain data relating flux and solenoid current prior to the tube-test. To accomplish this, the magnetic circuit was completely assembled and a magnetization curve taken, measuring flux density at the mean radius of the beam. Flux density was measured directly using a gauss-meter manufactured by the Dyna-Labs Corporation. At the center of the pole structure the calculated value of required flux density was 59 gauss. This corresponds to a total flux of 6.2 x 10^{-6} webers. Figure 4.4, the magnetization curve, shows that this density

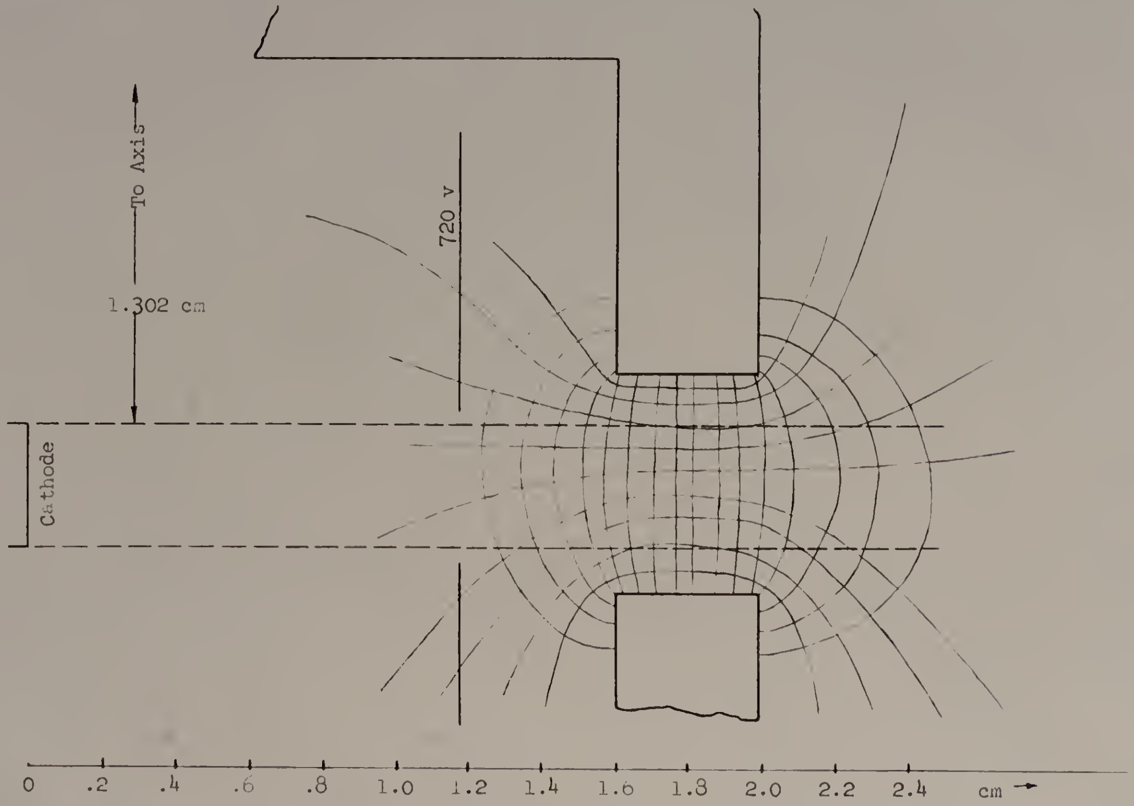

MAP OF THE MAGNETIC FIELD

FIGURE 4.2

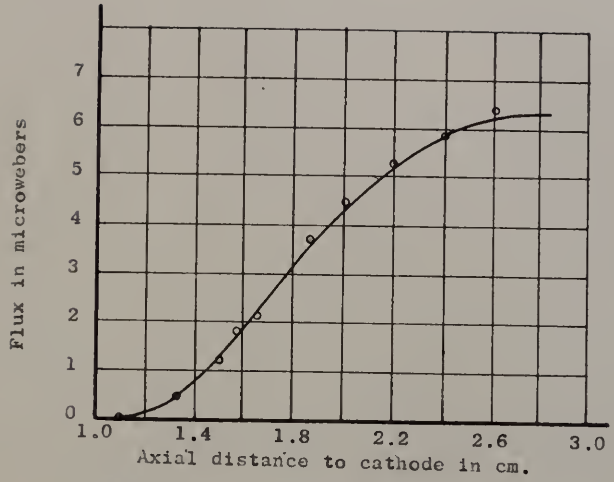

FLUX VS. AXIAL DISTANCE IN THE TRANSITION REGION

FIGURE 4.3

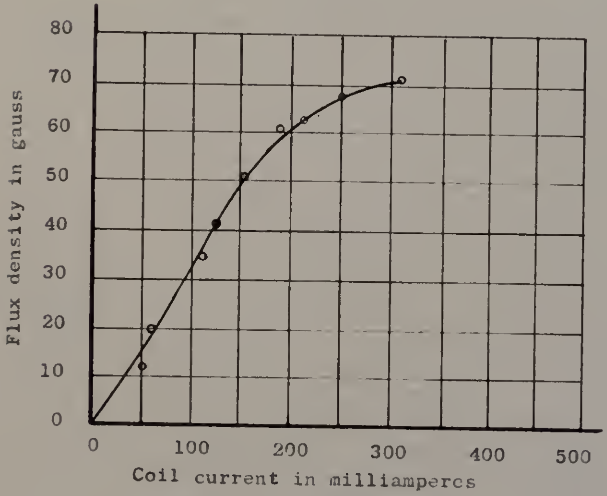

FLUX DENSITY VERSUS SOLENOID CURRENT

FIGURE 4.4

was obtained for 190 milliamperes in the solenoid.

The location of the pole pieces with respect to the cathode region was somewhat arbitrary. They had to be far enough away to keep flux out of the cathode region, but at the same time as near as practicable in order to shorten the over-all collimation length. The relative positions selected are shown on Figure 4.2 where the 720-volt electrode represents the extent of the cathode region.

Locating Electrodes in the Transition Region

Finding the location of electrodes in the transition region consisted of carrying out the net point procedure described in Chapter III and drawing equipotential surfaces to influence the entire region. The pole elements constituted surfaces of zero potential and had to be shielded by the electrode system.

In the design of the tube a multitude of potential values were calculated, corrected, and plotted in the neighborhood of the beam boundary. These calculations are not presented in their entirety, but for clarity a sample calculation is given here.

Consider Figure 4.5. The points pictured are located about halfway through the flux region. Along the outer beam radius the potential is 720 volts. Potential at the set of points along a radius of 1.69 centimeters is determined from equation 3.3.

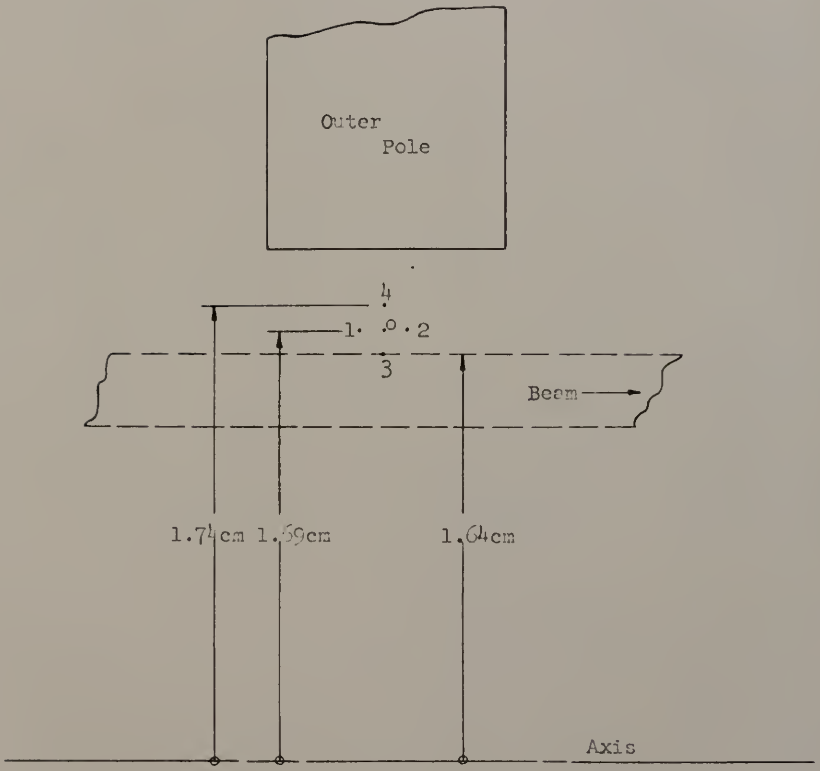

REPRESENTING POINTS USED IN SAMPLE CALCULATIONS

FIGURE 4.5

$$\emptyset_i = 720 + \frac{e}{m} \; \frac{h\,\Psi_i^{\,2}}{4\pi^2 r_o^{\,3}} \quad ,$$

where

$\emptyset_i$ is potential at the i^{th} point

Ψ_i is flux traversed at this point

$r_o = 1.69 \times 10^{-2}$ meters

$h = .05 \times 10^{-2}$ meters;

thus

$\emptyset_i = 720 - 4.6 \times 10^{11} \Psi_i^2$

At points 1, 0, and 2 respectively we find from Figure 4.3 that:

$\Psi_1 = 2.7 \times 10^{-6}$ webers

$\Psi_o = 3.05 \times 10^{-6}$ webers

$\Psi_2 = 3.41 \times 10^{-6}$ webers.

Corresponding potentials are:

$\emptyset_1 = 716.7$ volts

$\emptyset_o = 715.7$ volts

$\emptyset_2 = 714.7$ volts.

The potential at point 4 is found from equation 3.5.

$$\emptyset_4 = \frac{8r_o}{2r_o+h}\,\emptyset_o - \frac{2r_o}{2r_o+h}(\emptyset_1+\emptyset_2) - \frac{2r_o-h}{2r_o+h}\,\emptyset_3$$

$$= 3.94(715.7) - .984(1431.4) - .974(720)$$

$$= 710 \text{ volts.}$$

Calculations for values inside the beam were made similarly except that h was a negative increment of radius. In all, about four hundred potential values were determined. Figure 4.6 is a scale drawing showing the resulting net-point plot. The equipotential lines shown are those selected for focusing-electrode design. Notice that these lines become parallel to the beam after passing into the flux-free region. This means that in the drift-tube region the beam may be held in focus by a pair of coaxial cylinders, one inside and one outside the electron stream.

Description of Hollow Beam Electron Gun and Collimating Device

Figure 4.7 shows a scale drawing of the tube as actually constructed, and Figure 4.8 is a photograph of the tube and test set-up. The radial distances, in inches, to the important points on electrode surfaces are given next.

Axis to point D - .473 inches
E - .442 "
F - .485 "
G - .463 "
H - .461 "
I - .327 "
J - .490 "
K - .225 "
L - .490 "

Axis to point O - .512 inches
P - .623 "
R - .680 "
S - .720 "
T - .670 "
U - .725 "
V - .669 "
W - .905 "
X - .700 "

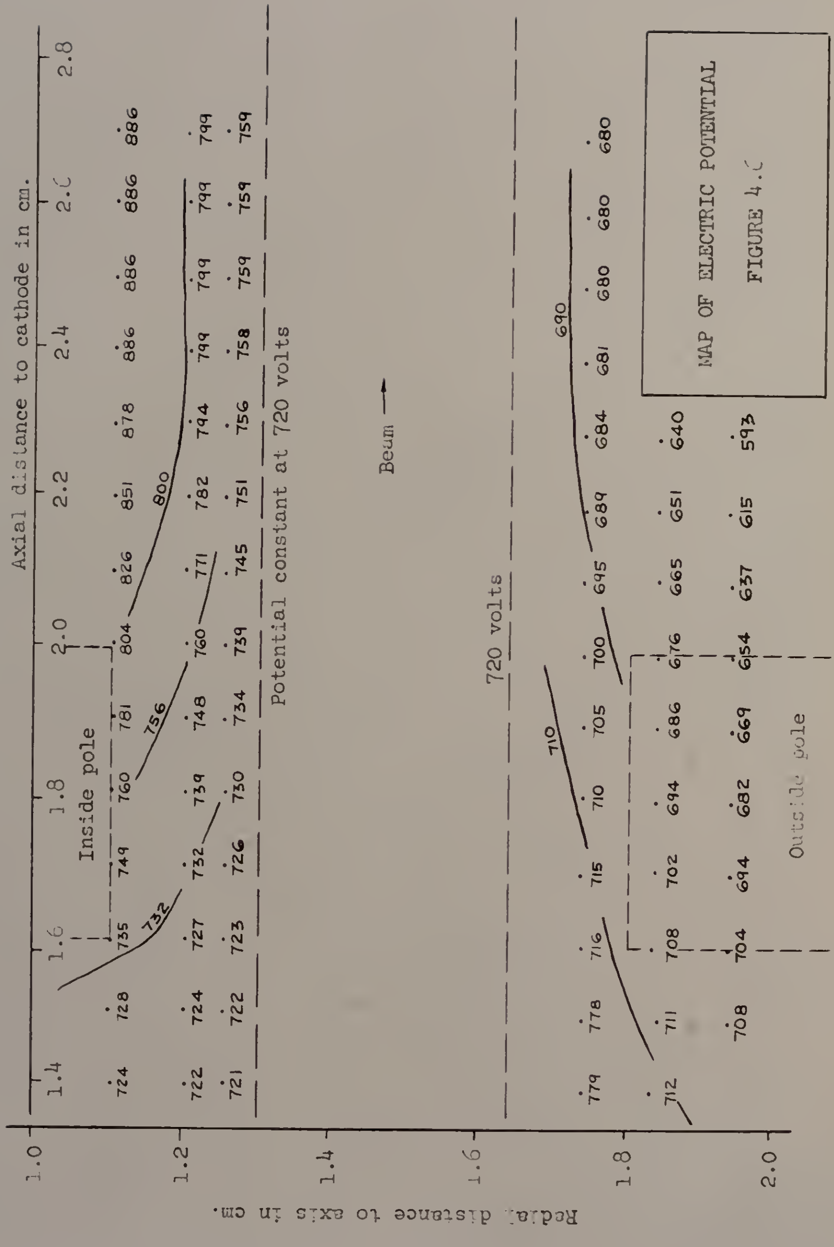

MAP OF ELECTRIC POTENTIAL

FIGURE 4.6

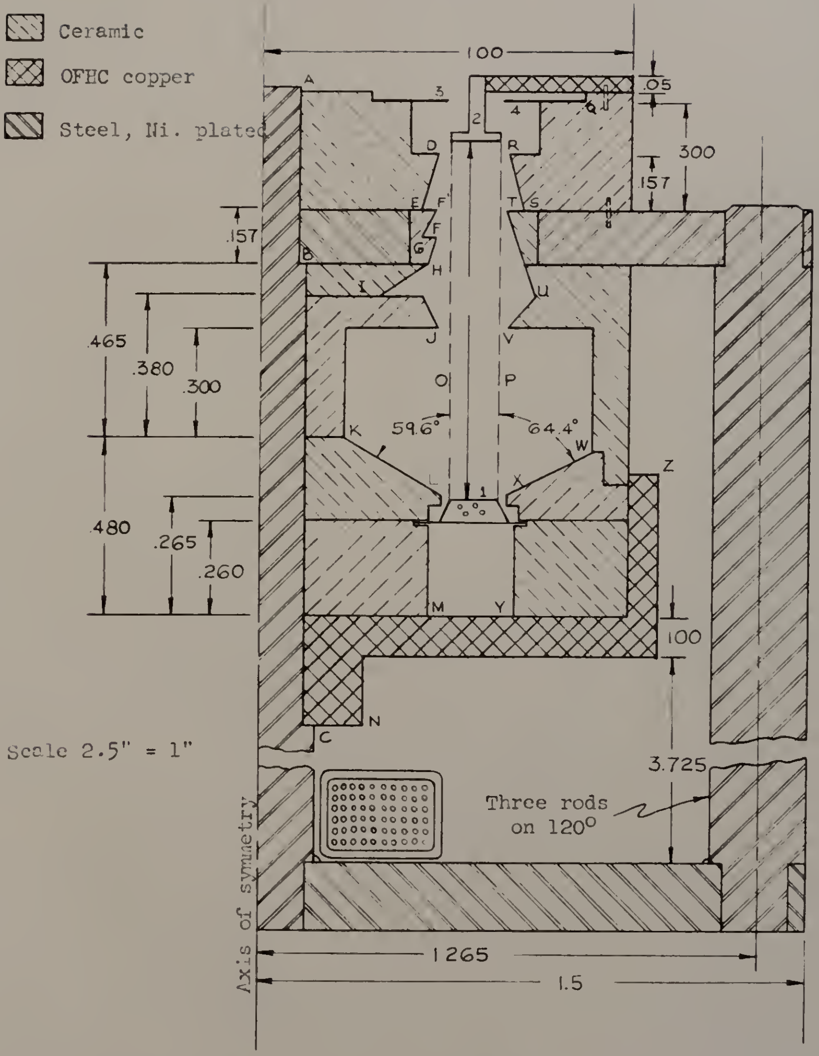

CROSS-SECTION OF THE HOLLOW BEAM ELECTRON GUN

FIGURE 4.7

This list serves to define slopes of the equipotential surfaces required by design calculations.

The magnetic circuit was of cold-rolled steel with nickel plating. The magnetic winding was sealed in a partially evacuated glass envelope to isolate it from the high vacuum.

The cathode cup and back plate were pressed separately from thin nickel sheet using special dies. One end of the heater element was spot welded to the back plate and the other end passed through a hole in the plate. The cup was then prepared for cathode coating using the C-1A process.[11] The oxide coating used for this cathode was prepared by the Sylvania Company. Prior to application the material, in suspension, was rolled slowly for about two hours. The cathode cup and back plate were then welded together and placed on a lathe for coating. The coating was applied by rotating the assembly against a fine camel-hair brush. Several applications were made, allowing each coat to dry under a heat lamp. Finally the surface was scraped, using a clean, sharp blade.

The heater for this cathode was made by winding .007" tungsten wire on a special jig with twin-spiral grooves cut in a plane. The heater was fired and coated by the Radio Corporation of America in their laboratories. This company and the Sylvania Company were very generous in furnishing these cathode materials gratis.

The ceramic parts shown in Figure 4.7 were machined from Lava, Grade 1137, furnished by the American Lava Corporation. This is a natural stone particularly suitable for high vacuum work. The electrode surfaces were created by painting the appropriate areas with Troy Burnish Silver Paste obtained from Hanovia Chemical and Manufacturing Company. The ceramic parts were hydrogen fired prior to silver-coating. The coating was then applied and cured in a slightly oxidizing atmosphere at 750°C, after which the pieces were again fired in a slightly reducing atmosphere.

Prior to hardening, minute holes were drilled in the ceramic parts to permit the passage of electrical leads. These holes terminate in the planes of the electrode surfaces. Leads of .010" OFHC copper were passed through these holes and attached to the silver coating using a very small plug of solder with high tin content. The solder was then melted with a clean iron creating a bond with the silver, and at the same time leaving the electrode surface perfectly flat.

Collimation of the beam was checked by measuring current to the beam collector, collector rings, and electrode surfaces. These tube elements are identified on Figure 4.7 according to Table 2. The beam collector was machined from nickel tubing and the collector rings were cut from molybdenum sheets.

Tube-Test Procedure and Results

The tube was tested in a demountable chamber evacuated by a three-stage, glass, oil-diffusion pump manufactured by Distillation Products Incorporated. The glass system included a cold-trap consisting of a pyrex finger one inch in diameter and about ten inches long. The metal base plate was sealed to the pump with Apiezon "W" wax. Pressures were measured using an RCA 1949 ionization gage. After more than twenty-four hours of continuous pumping a pressure of about 5 x 10^{-5} mm. of mercury was obtained. A dewar containing dry ice and acetone was placed on the cold trap and the system pressure dropped to 10^{-6} mm. of Hg. At this point activation of the cathode was attempted using, as a guide, the procedure outlined in the MIT Tube Manual.[11]

The rapid evolution of gas ceased at a heater power input of 30 watts. A small D.C. voltage was then applied to the accelerating electrode system, and current flow was noted. This was accompanied by an increase in pressure due to bombardment. The small current was maintained until vacuum conditions were again stable. This process was continued until the anodes were operating at rated voltage. A current of 50 milliamperes was observed.

At this stage of the test, potentials were applied to the other electrodes, and the magnetic circuit was energized. The following table is introduced to enable the reader to make cross-reference between tube elements shown on Figure 4.7 and Table 3 which presents tube-test data.

TABLE 2

TUBE ELEMENT IDENTIFICATION

Beam current collector	Element 2
Ring collector	Elements 3 and 4
Inside accelerator	Surface J
Outside accelerator	Surface V
Focus 732	Surface FHI
Focus 710	Surface TU
Focus 800	Surface DE
Focus 690	Surface RS
Focus 756	Surface F'G
Focus 0	Surfaces KL and WX

The accelerating electrodes (or anodes) drew a considerable current throughout the entire test. For instance, in run 7 (for which collimation was quite good) the current entering the transition region was only 23 milliamperes while anode current was 28 milliamperes. This behavior was to be expected, however, because the circular opening in the anode was quite small, the area being 3.14 square centimeters while total anode area was 16.6 square centimeters. Even though the focusing electrodes were designed to hold the beam to the gap area, it is not reasonable to expect that

TABLE 3

TUBE TEST DATA

Run Number	1	2	3	4	5	6	7	8	9
Beam current ma	0	4	6	8	4	13	17	16	23
Ring current ma	0	6	11	14	18	11	6	8	12
Inside anode current ma	32	26	18	14	13	13	15	14	9
Outside anode current ma	24	24	15	15	14	14	13	13	8
Focus 732 voltage volts	732	700	700	700	700	700	700	700	700
Focus 710 voltage volts	710	710	710	710	710	710	710	710	710
Focus 800 voltage volts	810	790	790	790	790	790	790	790	790
Focus 756 voltage volts	756	756	756	756	756	756	756	756	756
Focus 690 voltage volts	690	700	700	700	700	700	700	700	700

TABLE 3 (continued)

Inside anode voltage volts	720	720	720	720	720	720	720	720	710
Outside anode voltage volts	720	720	720	730	730	730	730	730	720
Focus 0 voltage volts	0	0	0	0	0	0	0	0	0
Beam collector voltage volts	720	720	720	720	720	720	720	720	730
Ring collector voltage volts	720	720	720	720	720	720	720	720	730
Flux density gauss	58	58	40	40	35	45	50	55	50

none of the current would be attracted to the existing parts of the accelerating system. The author believes a greater percentage through the gap could be realized by giving the surfaces KL and WX (see Figure 4.7) a greater slope, or by operating them at a slightly negative potential. Either procedure would establish a radial component of electric field away from the beam edges. This behavior was noted in the analog design of these surfaces. It was not possible to operate them at negative potential during the test because they were connected to the cathode internally.

Collimation within the cathode region proved to be quite satisfactory. Instruments connected in the leads to the focusing electrodes indicated zero current, or currents so slight as to be negligible. The measure of beam collimation by the transition region is made by comparing beam current with ring current. As depicted in Figure 4.7, the collector system consisted of a washer-shaped beam collector with two ring-collectors placed one-tenth of an inch further along the axis. The beam collector was located slightly beyond the final focusing electrode. Per cent collimation is defined as the ratio of beam current to total current entering the transition region times one hundred. This percentage value is a good measure of collimation because the area of the ring system was considerably greater than that of the beam collector. The former was

4.47 square centimeters and the latter 3.14 square centimeters. Table 4 presents collimation data for the test.

Note that runs 4 through 8 clearly indicate the degree of beam control available with the small radial field. For these runs beam potential was constant, focusing electrode potentials were held constant, and magnetic field values were varied. Run 5 indicates that for low flux density a considerable amount of current flowed to the inside ring collector. Strengthening the field gave a greater angular velocity to the constant energy electrons and increased the beam radius. This seems to be confirmed by the data observed in runs 6 and 7. Design information indicates that optimum collimation should occur with a pole-center flux density of 59 gauss. The data show best results for a density in the neighborhood of 50 gauss. It follows that as the flux was increased the beam radius became too large and a greater percentage of current flowed to the outer ring.

TABLE 4

COLLIMATION DATA

Run No.	Flux Density gauss	Beam Current ma	Ring Current ma	Per cent Collimation
1	58	0	0	----
2	58	4	6	40%
3	40	6	11	35.3%
4	40	8	14	36.4%
5	35	4	18	22.2%
6	45	13	11	54.1%
7	50	17	6	73.9%
8	55	16	8	66.6%
9	50	23	12	65.7%

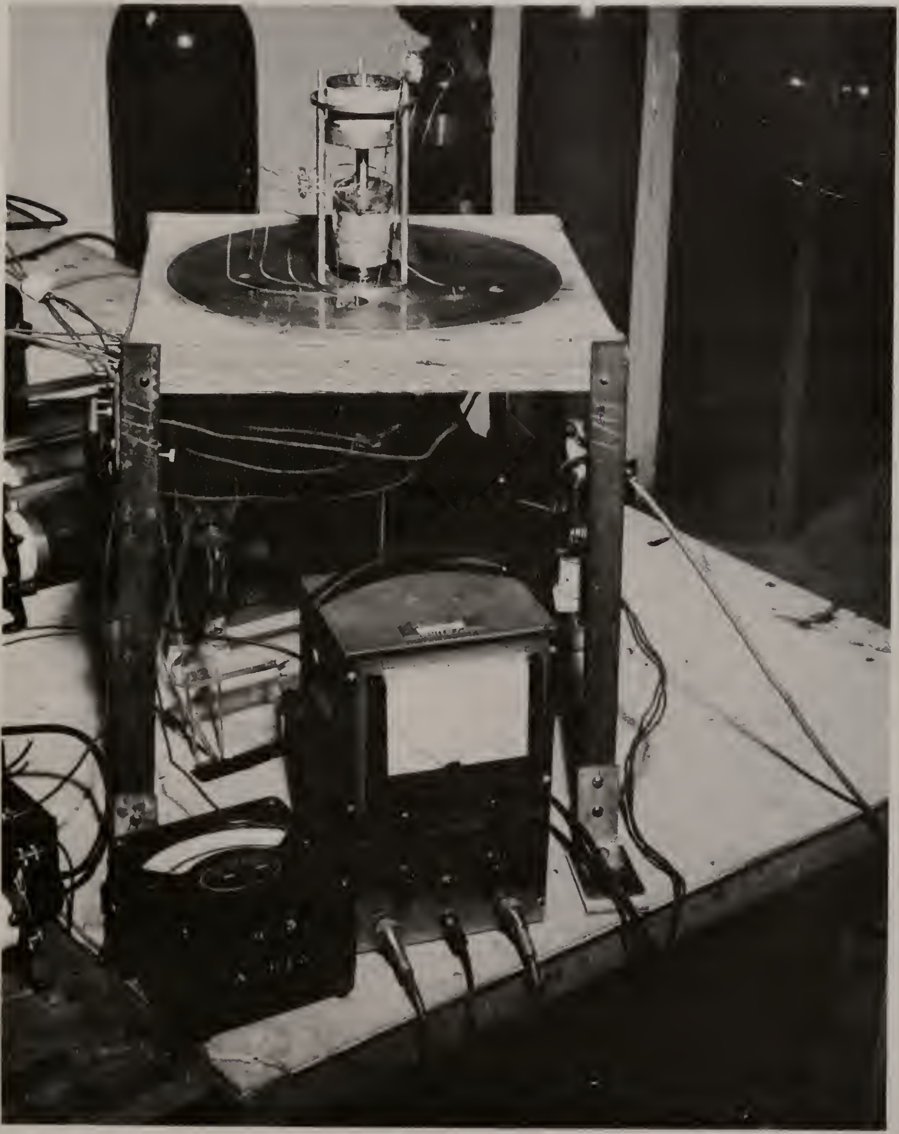

FIG. 4.8 -- THE ELECTRON TUBE AND TEST SET-UP

CHAPTER V

SUMMARY

In this work it has been demonstrated that a relatively dense hollow electron beam may be formed and controlled without the use of a strong axial magnetic field. Pierce's electron-gun technique proved to be quite successful in the cathode region design. This was to be expected, since all values were held within the known physical limitations of such beams. For instance, the perveance (defined as current divided by voltage to the 3/2 power) was 5.22×10^{-6} amperes per volt$^{3/2}$, a very moderate figure.

Another limitation in establishing dense beams is the formation of a virtual cathode somewhere along the beam. When the current is increased indefinitely, the depression of potential within the beam may be so great as to reduce the velocity of the inner electrons to zero, even though it is assumed that the beam boundaries remain fixed. As a result the current is limited. An equation derived by Calbick[14] has fixed the limiting value at $I = 29.3 \times 10^{-6} V^{3/2}$ amperes. This would permit a current of 575 ma in the tube discussed in the present work. Since

100 ma was the greatest value expected, the tube operated with a more than 500 percent margin on this limitation.

Chapter III presents a very workable method for finding focusing surfaces in the magnetic flux region. However, obtaining the required flux density in practice developed into a considerable problem, the difficulty being that the total flux necessary was so very small. It was required that the beam emerge from the transition region with an energy of 720 electron volts and with a ratio of tangential velocity to axial velocity of 1.55. (This requirement was based upon a practical pitch for a wound-helix, slow-wave guiding structure. The wave guide was to be wound on a ceramic core and operated within the hollow beam.) The above figures led to a tangential electron velocity of 1.34×10^7 meters per second. Substituting this velocity and a radius of 1.302×10^{-2} meters (the inner beam radius) in equation 2.25 gave 6.22×10^{-6} webers for the total flux. The resulting flux density at the center of the gap was found to be 59 gauss. This low density was difficult to obtain and difficult to measure accurately. However, performance of the tube when subjected to various flux densities in the neighborhood of 59 gauss definitely demonstrated that beam collimation was controlled by the weak radial field.

No good method for checking the pitch of the spiral trajectory of the beam was devised. Considerable thought was given to the possibility of getting a visible image of the beam on a screen coated with willemite. Had this been done, the cathode might have been marked causing a shadow to appear on the screen. The angular displacement of the shadow from the cathode scar would have furnished a measure of beam rotation. The author was advised against this technique, however, because of the relatively immense beam current.

It should be mentioned here that the design procedure deals only with the surface layers of the beam. Conditions for equilibrium of electrons at the inner and outer radii are presented. It is assumed that the trajectories do not cross radially, hence none of the internal electrons reach the surface boundaries with radial velocity components. This assumption may not be entirely correct, but there seems to be sufficient experimental justification for its use[15].

Figure 4.6 shows that the equipotential surfaces in the Laplace field region become coaxial cylinders after the beam emerges from the magnetic flux. Thus, in the drift-tube (traveling-wave section) space it should be possible to hold the electrons in collimation by a pair of coaxial electrodes, one within and one without the beam. The wound-helix referred to earlier might serve as the inner electrode if operated at a suitable D.C. potential.

Harris has presented[15] some experimental evidence supporting the above conjecture. This was not the primary purpose of his work, however, and further experimental work on this type of drift-tube would seem to be a very worthwhile project. The author is presently engaged in a continuation of the research reported here and hopes to gather considerable drift-tube data during the experimental phase of his study.

APPENDIX I

THE NET-POINT EQUATION

Equation 3.4 results from a consideration of the difference form of Laplace's Equation in cylindrical coordinates. For the axially symmetric potential field surrounding the beam, Laplace's equation is:

$$\frac{\delta^2\emptyset}{\delta r^2} + \frac{\delta^2\emptyset}{\delta z^2} + \frac{1}{r}\,\frac{\delta\emptyset}{\delta r} = 0 \ .$$

Consider Figure 3.5. At point 1 the partial derivative of potential with respect to r is given approximately by the relation:

$$\left(\frac{\delta\emptyset}{\delta r}\right)_1 \approx \frac{\emptyset_c - \emptyset_a}{2h} \ .$$

The second partial derivative with respect to r at this point is:

$$\left(\frac{\delta^2\emptyset}{\delta r^2}\right)_1 \approx \frac{1}{h}\left[\frac{\emptyset_c - \emptyset_1}{h} - \frac{\emptyset_1 - \emptyset_b}{h}\right] .$$

Similarly,

$$\left(\frac{\delta^2\emptyset}{\delta z^2}\right)_1 \approx \frac{1}{h}\left[\frac{\emptyset_d - \emptyset_1}{h} - \frac{\emptyset_1 - \emptyset_b}{h}\right] .$$

Substituting these values in Laplace's equation we obtain

$$\frac{1}{h}\left[\frac{\phi_c-\phi_1}{h} - \frac{\phi_1-\phi_a}{h}\right] + \frac{1}{h}\left[\frac{\phi_d-\phi_1}{h} - \frac{\phi_1-\phi_b}{h}\right] + \frac{1}{r_1}\left[\frac{\phi_c-\phi_a}{2h}\right] = 0 .$$

Collecting terms and solving for ϕ_1 yields the net-point equation,

$$\phi_1 = \frac{1}{4}(\phi_a + \phi_b + \phi_c + \phi_d) + \frac{h}{8r_1}(\phi_c - \phi_a). \qquad (3.4)$$

The method of application of the above equation depends upon the available boundary information. The value of the potential at a point in a charge-free space is the average of the potentials of all points equidistant from it. Then if the potential of a sufficient number of boundary points is known, one may make a judicial guess at values for the remainder of the net-points. The assigned values may then be used to calculate a more nearly correct set of potentials. This process, which is known as the relaxation method,[12] should be repeated several times until further repetitions yield no change. That the procedure is a convergent one has been definitely established. See, for instance, reference 13.

The application of this method in the present work is rendered easier by a knowledge of the electric field intensity as well as potential at the beam boundary. With this information it is possible to calculate values at points immediately adjacent to the boundary leaving only one value unknown in equation 3.4. This procedure is discussed in the section on Approach to Transition Region Design.

APPENDIX II

ON THE ELECTROLYTIC TANK ANALOGY

The analytical solution to Laplace field problems is limited to cases having only the simplest boundaries. In applications where the boundaries cannot easily be expressed mathematically solutions become difficult or impossible. Solutions to such problems are often found by making use of the electrolytic tank analogue. This method was first used by Fortescue[16] in 1913 and has since become a very familiar scientific tool. Many complete treatments of the theory and application of the tank are to be found in literature. The reader is referred, for instance, to Volume I of Electromagnetic Fields by Weber[10] or to Electron Optics by Coslett[17]. These remarks are included as an immediate reference and as an extension of the discussion in Chapter III.

Consider a pair of electrodes in free space with a source of electric potential connected between them. Consider, also, a similar system with the electrodes immersed in a homogeneous, slightly-conducting liquid. In the former case lines of electric flux permeate the space, and in the latter case current flow lines pass through the electrolyte. In both cases electric fields exist in the regions about the electrode arrangements. These are vector fields and are, by definition, proportional to the gradient of potential. It is now shown that each of the potential functions satisfies Laplace's equation.

Potential in the Electrostatic Field
Around the Electrodes

It is presumed that no charge exists in the region about the electrodes in space. By definition

$$E = -\nabla \phi, \qquad \text{(II-1)}$$

where E is the electric field and ϕ is the potential. Since an electric flux line must originate or terminate on charge and inasmuch as charge is absent, this field has no divergence. Expressed mathematically, this states that

$$\nabla \cdot E = 0. \qquad \text{(II-2)}$$

Combining equations II-1 and II-2 yields Laplace's equation.

$$\nabla \cdot E = -\nabla \cdot (\nabla \phi) = 0$$

or

$$\nabla^2 \phi = 0. \qquad \text{(II-3)}$$

Potential in the Electrolyte Around the Electrodes

The electrolyte permits current to flow. At any point within the liquid the current density is proportional to the electric field and is given by

$$J = \gamma E, \qquad \text{(II-4)}$$

where J is current density and γ is conductivity. The current density vector obeys the equation of continuity,

$$\nabla \cdot J = -\frac{\delta \rho}{\delta t}, \qquad \text{(II-5)}$$

where ρ is volume charge density. Since as much charge flows out of any volume element as flows into it, the partial derivative of ρ with respect to time is zero, and the divergence of the current density is zero.

$$\nabla \cdot J = 0. \qquad \text{(II-6)}$$

Substituting equation II-4 into II-6 yields the following:

$$\nabla \cdot E = 0. \qquad \text{(II-7)}$$

Again E is the negative of the gradient of a potential field. It is significant that, in this instance, the difference of potential from point to point is created by an IR drop. Let this potential be designated by the symbol V. Thus $E = -\nabla V$ and equation II-7 becomes

$$-\nabla \cdot (\nabla V) = 0$$

or

$$\nabla^2 V = 0. \qquad \text{(II-8)}$$

Equation II-8 is Laplace's equation, and the IR drop field in the electrolyte is seen to be exactly analogous to the electrostatic potential field. The importance of all this lies in the fact that the IR drop can be measured whereas the other potential cannot. A description of a typical electrolytic tank application may be found in Chapter III.

APPENDIX III

ON FLUX PLOTTING

Besides the electrolytic tank analogue another good way of making a field study is the graphical flux plot. A magnetic field is chosen to illustrate the method.

Refer to Figure III-1 which depicts a flux tube within the field. The tube is bounded such that its walls inclose the same total flux, $\Delta\Psi$, from beginning to end. The surfaces normal to the flux direction represent magnetic equipotentials, U_1, U_2, and U_3. Assume that there are no variations with respect to x, and that spacing is chosen to require equal potential differences between adjacent surfaces. Let the following table of symbols apply.

H - Magnetic field intensity

B - Magnetic flux density

μ - Permeability

Δs - Spacing of equipotential surfaces

$\Delta \ell$ - Height of flux tube

Now the potentials U_3 and U_2 may be expressed as follows:

$$U_3 = U_2 + H_2 \Delta s_2 \qquad \text{(III-1)}$$

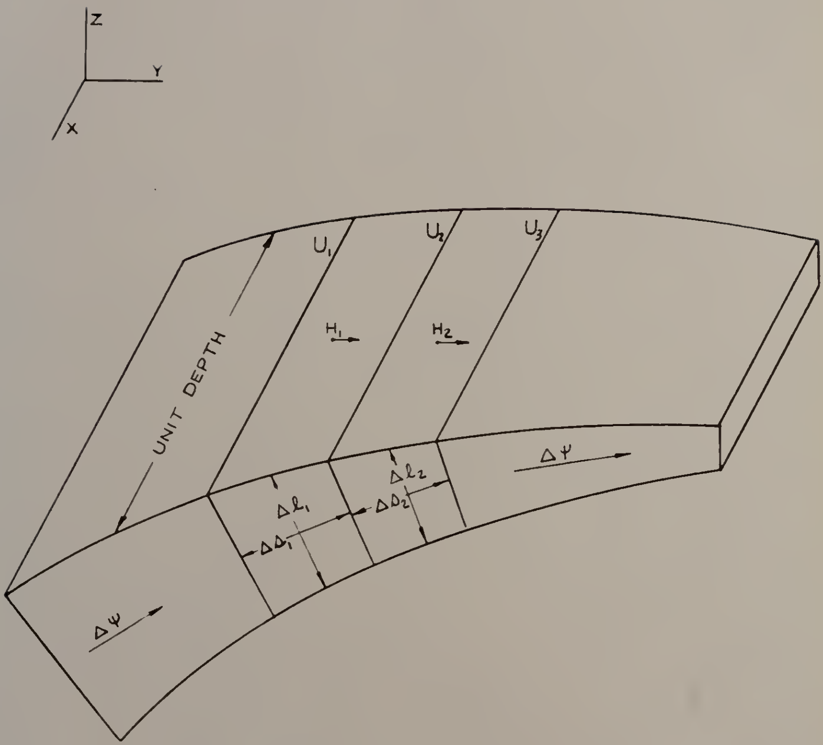

FLUX TUBE CONDUCTING A SMALL QUANTITY OF MAGNETIC FLUX

FIGURE III - 1

and

$$U_2 = U_1 + H_1 \Delta s_1 . \qquad \text{(III-2)}$$

Subtracting equation III-2 from III-1 yields

$$U_3 - U_2 = U_2 - U_1 + H_2 \Delta s_2 - H_1 \Delta s_1 . \qquad \text{(III-3)}$$

But since $U_3 - U_2 = U_2 - U_1$ it is seen that

$$H_1 \Delta s_1 = H_2 \Delta s_2 . \qquad \text{(III-4)}$$

Let H now be expressed in terms of the flux within the tube.

$$H = \frac{1}{\mu} B = \frac{1}{\mu} \frac{\Delta \Psi}{1 x \Delta \ell} . \qquad \text{(III-5)}$$

Substituting this in equation III-4 yields

$$\frac{\Delta s_1}{\Delta \ell_1} = \frac{\Delta s_2}{\Delta \ell_2} \qquad \text{(III-6)}$$

Thus, spacing of equipotentials is also a measure of the height of the flux tube. Then if families of orthogonal curves are drawn in the y-z plane such that they form curvilinear squares in that plane and satisfy boundary conditions of the potential, the result is a plot of flux flow lines and equipotential lines. The latter generate surfaces when translated parallel to the x-axis.

The above discussion is for two-dimensional fields, but with only slight modification is applicable to fields having axial symmetry. The graphical solution to any field problem is rendered easier by making use of all available information. For instance, equipotential surfaces are parallel to boundary potentials near the boundaries. Also, quite frequently, either flow lines or equipotential lines will follow lines of symmetry.

The magnetic field problem encountered in this work was that of finding flux distribution. Magnetic potential distribution was not needed. However, in order to reduce the tedious work of flux plotting to a minimum, a model of the magnetic system was set up in the electrolytic tank and data providing equipotential lines were taken. Then there remained only to sketch in the orthogonal family of flux lines. Thus it is sometimes possible (and desirable) to combine these methods of field solution.

BIBLIOGRAPHY

1. Samuel, A. L., Proc. I.R.E., vol. 37, pp. 1252-58; November 1949.
2. Wang, C. C., Proc. I.R.E., vol. 38, pp. 135-147; February 1950.
3. Pierce, J. R., Jour. Appl. Phys., vol. 10, pp. 715-724; October 1939.
4. Wax, N., Jour. Appl. Phys., vol. 20, pp. 242-248; March 1949.
5. Harris, L. A., Proc. I.R.E., vol. 40, pp. 700-708; 1952.
6. Pierce, J. R., Theory and Design of Electron Beams, D. Van Nostrand Company, Inc., New York, 1954.
7. Spangenberg, K. R., Vacuum Tubes, McGraw-Hill Book Company, New York, 1948.
8. Killer, L. R., The Physics of Electron Tubes, McGraw-Hill Book Company, New York, 1937.
9. Goldstein, Herbert, Classical Mechanics, Addison-Wesley Press, Inc., Cambridge 42, Massachusetts, 1951.
10. Weber, Ernst, Electromagnetic Fields, vol. I, John Wiley & Sons, Inc., New York, 1950.
11. Tube Laboratory Manual, Research Laboratory of Electronics, M.I.T., Cambridge, Massachusetts, 1951.
12. Southwell, R. V., Relaxation Methods in Theoretical Physics, Oxford University Press, England, 1946.
13. Bateman, H., Partial Differential Equations of Mathematical Physics, Dover Publications, New York, 1944.
14. Calbick, C. J., Bulletin of the American Physical Society, vol. 19, No. 2, p. 14; April 1944.

15. Harris, L. A., Axially Symmetric Electron Beam and Magnetic Field Systems, Technical Report No. 170, M.I.T., Cambridge, Massachusetts, 1950.

16. Fortescue, C. L. and Farnsworth, S. W., Trans. A.I.E.E., vol. 32, p. 893; 1913.

17. Cosslett, V. E., Electron Optics, Oxford at the Clarendon Press, England, 1950.

BIOGRAPHY

Leonard Caldwell Adams was born in Saluda, South Carolina on November 7, 1921. He began his undergraduate program at Clemson College in Clemson, South Carolina in 1939 and received the degree of Bachelor of Electrical Engineering in 1943.

In 1950 he received the degree of Master of Science in Electrical Engineering from the Oklahoma Institute of Technology at Oklahoma A. & M. College. In the summer of 1951 Mr. Adams began work leading to the degree of Doctor of Philosophy with a major in electrical engineering at the University of Florida.

From 1943 to September of 1946 Mr. Adams served in the A.U.S. At the time of separation he was an officer in the Signal Corps. Since 1946 he has been on the staff of the Electrical Engineering Department at Clemson College except for various leaves of absence during which he pursued graduate work at Oklahoma A. & M. and at the University of Florida. During these graduate programs Mr. Adams held teaching and research assistant positions.

He is a member of Tau Beta Pi, Phi Kappa Phi, Eta Kappa Nu, Sigma Xi, and The Institute of Radio Engineers.